PCCP

Accepted Manuscript

This article can be cited before page numbers have been issued, to do this please use: L. J. Mendoza Herrera, I. J. Bruvera, L. B. Scaffardi and D. C. Schinca, *Phys. Chem. Chem. Phys.*, 2016, DOI: 10.1039/C6CP08260B.

View Article Online
DOI: 10.1039/C6CP08260B

Sizing and Eddy currents in magnetic core nanoparticles: an optical extinction approach †

Luis J. Mendoza Herrera,[a] Ignacio J. Bruvera[a] Lucía B. Scaffardi[a,b] and Daniel C. Schinca[a,b]

Optical extinction, is a handy and ubiquitous technique that allows to study colloidal nanoparticles in their native state. The typical analysis of the extinction spectrum can be extended in order to obtain structural information of the sample such as size distribution of the cores and thickness of the coating layers. In this work the extinction spectra of Fe_3O_4, Fe_3O_4@Au and Fe_3O_4@SiO_2@Au single and multilayer nanoparticles are obtained by solving full Mie theory with a frequency dependent susceptibility derived from Gilbert equation and considering the effect of Eddy currents. The results are compared with non magnetic Mie theory, magnetic dipolar approximation and magnetic Mie theory without Eddy currents. The particle size-wavelength ranges of validity of these different approaches are explored and novel results are obtained for Eddy current effects in optical extinction. These results are used to obtain particles size and shell thickness information from experimental extinction spectra of Fe_3O_4 and Fe_3O_4@Au nanoparticles with good agreement with TEM results, and to predict the plasmon peak parameters for Fe_3O_4@SiO_2@Au three layer nanoparticles.

1 Introduction

Iron oxide, gold and multilayer nanoparticles (NPs) are being studied with increasing enthusiasm in the last couple decades for their multiple applications in biomedicine.[1 2 3] Particles with magnetic properties can be used for drug delivery and targeting[4 5], gene and virus transfer (magnetofection)[6 7], magnetic resonance contrast[8 9] and oncological hyperthermia[10]. In all this biomedical applications, avoiding particle agglomeration is a critical goal in order to enhance in vitro and in vivo sample stability. In this direction, silica coating of magnetic NPs is a commonly visited tactic[11 12 13]. Gold coated NPs, for their part, are been extensively studied for their application in biomolecular sensors for diagnosis.[14 15]

Combinations of this and similar elements in multilayer NPs of controlled size could be used to obtain multitasking materials which can perform a sum of the previously mentioned functions or enhance the effect of one of the layers.[16 17 18]

Spherical NPs with a Fe_3O_4 magnetite core, coated with a SiO_2 silica shell and an external gold layer (Fe_3O_4@SiO_2@Au) are of special interest due their optical and magnetic properties acting in two clearly separated wavelength ranges. There is a compromise between the radii of each layer: the larger the magnetite core, the stronger the magnetic response of the particles but the size dependent optical extinction is affected by any size modification. Therefore, a theoretical understanding of the dependence of optical extinction with each layer size becomes important.

Mie theory is the most general formalism for the modelling of optical extinction of small particles. The precision of the results depend on the number of multipolar terms considered in the calculations. For non magnetic particles only the electric interaction is considered via the dependence with frequency of the permittivity $\varepsilon(\omega)$, while the susceptibility is fixed to $\mu = 1$.

In order to consider magnetic effects on the extinction, Draine & Hensley presented a model for MNP in interstellar medium in which they add a dipolar magnetic term to the non magnetic Mie theory with $\mu = 1$.[19] However, a more precise description of the extinction requires the explicit consideration of the magnetic contribution by the dependence with frequency of the susceptibility $\mu(\omega)$. In order to obtain $\mu(\omega)$ it is necessary to solve Gilbert equation, which depends on a parameter α_G that must be known for each material. If the particles are made of a conducting substance, the effect of Eddy currents must be taken into account also, as Draine and Hensey did in the cited work. These effects become important for a particle size range that must be determined for each material by comparison with non Eddy including models.

On the other hand, being the extinction also a function of particle size, the size distribution of real samples determine its experimental optical response. So in the opposite direction, it is possible

[a] Centro de Investigaciones Ópticas (CIOp),(CONICET La Plata-CIC), Cno. Parque Centenario e/ 505 y 508 Gonnet. C.C. 3 (1897) Gonnet, Buenos Aires, Argentina. Fax: int. 239; Tel: +54(221)484-0280/2957 ; E-mail: daniels@ciop.unlp.edu.ar
[b] Departamento de Ciencias Básicas, Facultad de Ingeniería, UNLP, Argentina.

† Electronic Supplementary Information (ESI) available: [details of any supplementary information available should be included here]. See DOI: 10.1039/b000000x/
‡ These authors contributed equally to this work.

View Article Online
DOI: 10.1039/C6CP08260B

to retrieve the size distribution of a sample from its measured optical extinction. There exist several other techniques allowing to obtain this information e.g. TEM and SAXS. Each one of these techniques present a different set of pros and cons referring to their statistical and environmental representativity, model dependency, amount of required sample and (the most important in some cases) availability. Then, optical extinction, being a cheap, ubiquitous technique, requiring small sample quantities (very diluted suspensions) and permitting the analysis of the particles in its native state, presents a very practical alternative for the size characterization of nanoparticle suspensions.

In this work, theoretical extinction spectra for Fe_3O_4, Fe_3O_4@Au and Fe_3O_4@SiO_2@Au NPs are obtained by solving full Mie theory with a frequency dependent susceptibility $\mu(\omega)$ derived from Gilbert equation and considering the effect of Eddy currents. The Gilbert parameter α_G for magnetite was obtained by fitting experimental extinction data.

The results are compared with non magnetic Mie theory, Draine & Hensley approximation and magnetic Mie without Eddy currents. The particle size and wavelength ranges of validity of the different models are explored and novel results are obtained for Eddy current effects in optical extinction.

Finally, these results are used to obtain particles size and shell thickness information from experimental extinction spectra of Fe_3O_4 and Fe_3O_4@Au with good agreement with TEM results, and to predict the plasmon peak parameters for Fe_3O_4@SiO_2@Au three layer nanoparticles.

2 Magnetic nanoparticles permeability from Gilbert equation

High magnetic moment materials, as Fe_3O_4, present a strong dependence of its permittivity and permeability with frequency. In order to study this dependencies, it is necessary to solve Gilbert equation

$$\frac{d\mathbf{M}}{dt} = \gamma \mathbf{M} \times \mathbf{H}_T + \alpha_G \frac{\mathbf{M}}{|\mathbf{M}|} \times \frac{d\mathbf{M}}{dt} \qquad (1)$$

where $\mathbf{M}$ is the magnetization, $\gamma = -ge/(2m_e c)$ is the magnetic moment/angular moment ratio, $g = 2$ is the giromagnetic factor, α_G is the Gilbert parameter and H_T is the total effective field.

Magnetite Fe_3O_4 has an ordering temperature T_N =860 K and a room temperature saturation magnetization M_s=90 Am^2/kg .[20 21] This compound has a cubic inverse spinel structure where two thirds of the iron ions are Fe^{3+}. Half of these ions occupy A sites (tetrahedral sites) and the other half occupy B sites (octahedral sites). The remaining third Fe ions are Fe^{2+} and occupy B sites. Since the antiparallel Fe_A^{3+} and Fe_B^{3+} moments compensate each other, a saturation magnetization of $m_A + m_B = 4\mu_B$ f.u. (formula unit) is expected from the remaining Fe_B^{2+} moments.

For an AC field $\mathbf{h} = h_0 e^{i\omega t}$ considering circular polarization, the final expression for the permeability results in

$$\mu(\omega) = 1 + \frac{12\pi(\chi_+ + \chi_-)}{9 - 4\pi(\chi_+ + \chi_-)} \qquad (2)$$

where

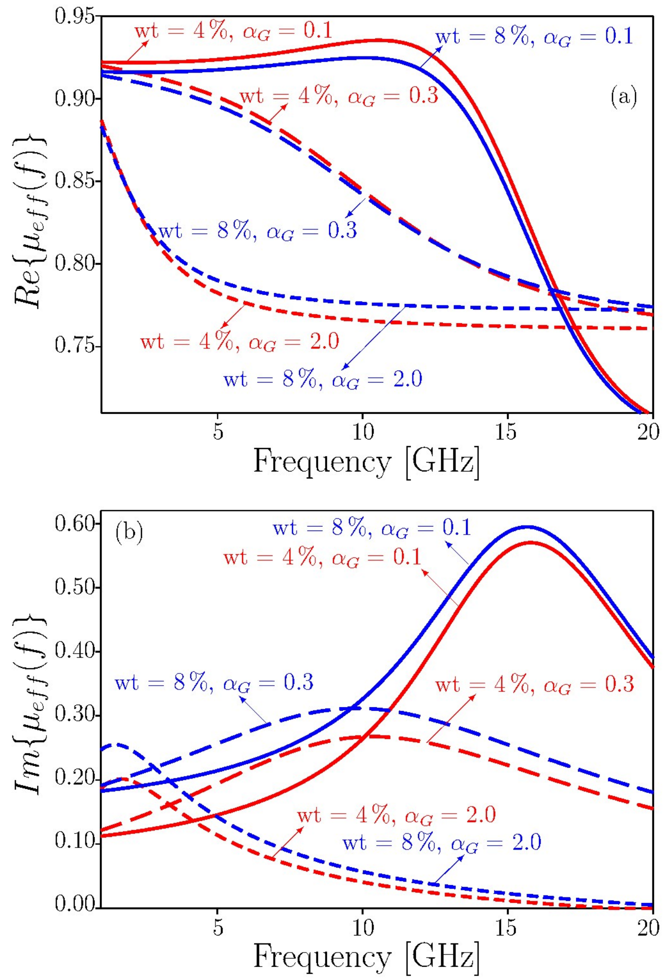

Fig. 1 Real (a) and imaginary (b) effective magnetic permeability of the NP@TPNR composite for several values of Gilbert parameter (α_G=0.1, 0.3, 2.0) and two NP concentrations (4 wt% and 8 wt%).

$$\chi_\pm = \frac{2N_{AB}\omega_{MA}\omega_{MB} - \omega_{MA}\omega'_{0B} - \omega_{MB}\omega'_{0A} \pm (\omega_{MA} + \omega_{MB})\,\omega}{N_{AB}^2\omega_{MA}\omega_{MB} - \omega'_{0A}\omega'_{0B} - \omega^2 \pm (\omega'_{0A} + \omega'_{0B})\,\omega} \qquad (3)$$

with $\omega'_{0A} = \omega_{0A} + i\alpha_G$ and $\omega'_{0B} = \omega_{0B} - i\alpha_G$. The values of ω_{0A}, ω_{0B} , ω_{MA}, ω_{MB} and N_{AB} in equation (3), can be found in the work of Draine & Hensley.

The value of parameter α_G for magnetite must be obtained from experimental extinction data. Kong *et al*[22] determine experimentally the effective magnetic permeability μ_e of a composite of NPs in thermoplastic natural rubber (TPNR) for three concentrations (4 wt%, 8 wt% and 12 wt%).This results can be used for the determination of α_G.

The extended Bruggeman effective permeability description[23 24] is given by

$$p\frac{A\mu_i - \mu_e}{A\mu_i + 2\mu_e} = (p-1)\frac{\mu_m - \mu_e}{\mu_m + 2\mu_e} \qquad (4)$$

where p is the volume fraction of magnetic NPs, μ_i the particles permeability, μ_m the medium permeability, μ_e the effective permeability and A is the parameter

View Article Online
DOI: 10.1039/C6CP08260B

$$A = 2\frac{ka\cos ka - \sin ka}{\sin ka - ka\cos ka - k^2a^2\sin ka} \quad (5)$$

with the wave number

$$k = [1+i]\left(\frac{\pi f \mu_i}{\rho \varepsilon_0 c^2}\right)^{1/2} \quad (6)$$

where f is the frequency, ρ the electrical resistivity and a the NP radius. Using equations (2) to (6), the effective permeability of the composites may be modeled as a function of α_G and wt%.

Figure 1 shows the results for the real and imaginary parts of the permeability of the NP@TPNR composite for two different concentrations (4 wt% and 8 wt%) and several α_G values (0.1, 0.3 and 2.0). The NPs characterized by Kong present radii in the range [20, 30] nm.

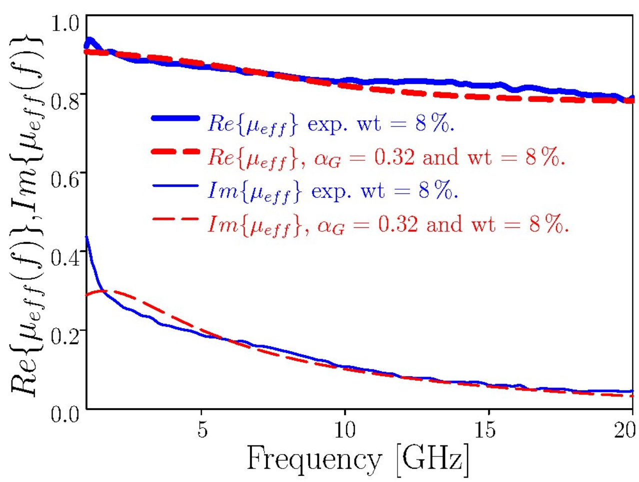

Fig. 2 Comparison between experimental data (full lines) and theoretical calculation (dashed lines) of the magnetite effective magnetic permeability for 8 wt% and α_G=0.32.

The actual value of α_G for each of the three concentrations was obtained by least squares between the experimental data points and the results of the calculations. The resulting mean of 0.32 will be used in the rest of this work. Figure 2 shows the comparison between experimental and calculated values for 8 wt%. It can be seen that there is a very good agreement between experimental data and theoretical calculation obtained for real and imaginary parts of the magnetite effective magnetic permeability in the range [1, 20] GHz.

3 Eddy Currents in nanoparticles

The polarizability due to induced currents depends on the relation between particle size and wavelength. So, in order to predict the optical response of a NP assemble, it is necessary to determine the size and wavelength ranges for which Eddy currents must be taken into account.[19 25]

3.1 Magnetic nanoparticles extinction

Extinction of magnetic nanoparticles was calculated by Draine & Hensley as the sum of two parts: the electric contribution C^{TM}_{abs} from the Mie theory with $\mu = 1$ and a dipolar magnetic contribution including Eddy currents.

The dipolar magnetic moment of a particle of volume V is $\mathbf{p}_m = V\mathbf{m} = \alpha_m \cdot \mathbf{h}$, where $\mathbf{m}$ is the magnetization and α_m is the magnetic polarizability tensor resulting from the sum of the magnetic contribution α^{mag} and the Eddy currents polarizability α^{Eddy}. For a conducting non magnetic sphere of radius a, the Eddy contribution is a diagonal tensor[25] with elements given by:

$$\alpha^{Eddy} = \frac{3V}{8\pi}\left[\frac{3}{y^2} - \frac{3}{y}\cot y - 1\right] \quad (7)$$

where $y^2 = \varepsilon\omega^2 a^2/c^2$.

For a finite conductivity, Eddy currents are not confined to the surface of the particle so, the magnetic field in the volume is not homogeneous.[19] The dipolar magnetic contribution takes the form

$$\alpha^{mag}\left(1+\frac{8\pi\alpha^{Eddy}}{3V}\right)V\left(\chi_+\mathbf{h}_+\mathbf{h}_+^* + \chi_-\mathbf{h}_-\mathbf{h}_-^*\right) \quad (8)$$

where $\mathbf{h}_\pm = (\mathbf{x} \pm i\mathbf{y})/\sqrt{2}$.

In this work another approach was taken, based on the calculation of the extinction by using full Mie theory with frequency dependent permittivity and permeability, plus an Eddy current contribution.

For a spherical particle of radius R, the efficiency is $Q_k = \frac{C_k}{\pi R^2}$ where C_k is the corresponding cross sections. Using the Mie expressions for the magnetic and electric fields in each region, the scattering and extinction efficiencies can be expressed as

$$Q_{scat} = \frac{2}{k^2c^2}\sum_{n=1}^{\infty}(2n+1)(|a_n|^2+|b_n|^2) \quad (9)$$

$$Q_{ext} = \frac{2}{k^2c^2}\sum_{n=1}^{\infty}(2n+1)\mathrm{Re}(a_n+b_n) \quad (10)$$

where c is the NP external radius and a_n and b_n expressions can be obtained from the fields border conditions in every region of the particles. These factors end up depending on the NPs radius and the permeability and conductivity of the materials. Permeability and conductivity depend at the same time on wavelength and NP size.

Figure 3 shows the extinction efficiency results corresponding to the different approximations mentioned above, for several NPs sizes. Mie theory with constant permeability $\mu = 1$ ($Q^{Mie}_{ext}(\mu = 1)$), and Mie theory with frequency dependent permeability $\mu(\omega)$ ($Q^{Mie}_{ext}(\mu(\omega))$) are compared with constant μ Mie theory plus the magnetic dipolar contribution (considered as the sum of magnetic and Eddy contributions) and Mie with $\mu(\omega)$ theory plus Eddy contribution. As the figure shows, the frequency dependent susceptibility consideration becomes important for long wavelengths (longer for larger particles) but it can be replaced by the magnetic dipolar correction with identical results. Only the $\mu = 1$ with no magnetic dipolar correction curve (black dashed line) presents a separated behavior for long wavelengths.

Eddy currents on the other hand, are irrelevant for small particles (d<20nm) while for large particles become important at short wavelengths as shown in the zoomed section of the fig-

View Article Online
DOI: 10.1039/C6CP08260B

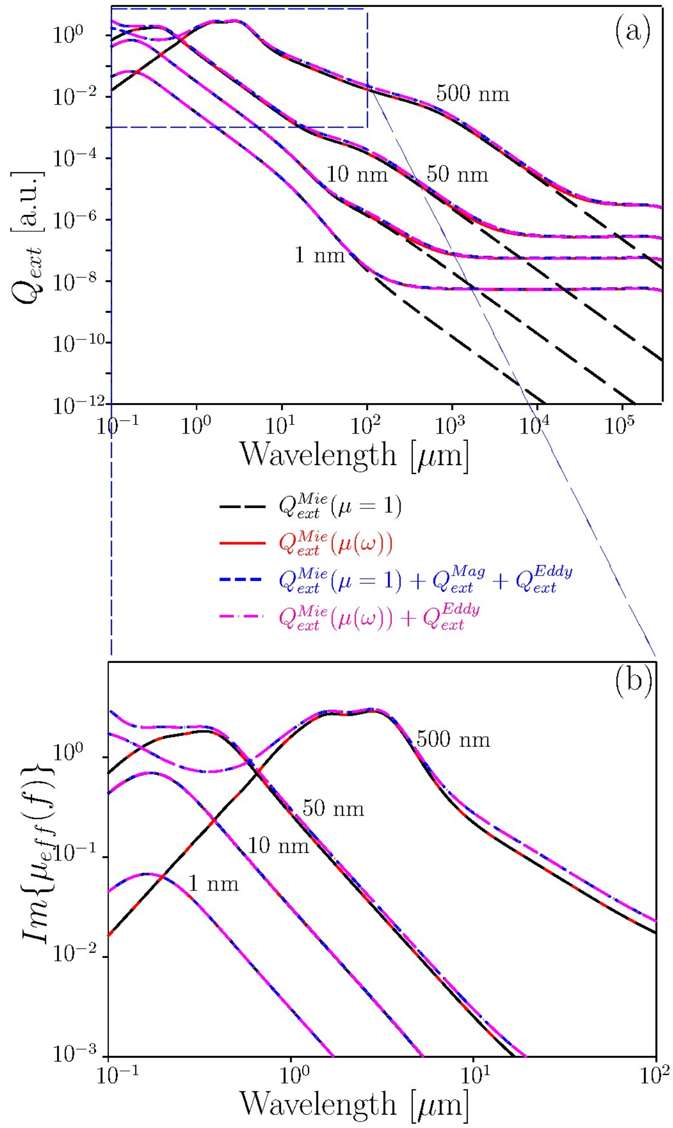

Fig. 3 (a) Comparison between extinction efficiencies predicted by the considered models. In black dashed line, the simpler approximation with constant permeability $\mu=1$. In red solid line, the frequency dependent permeability model with $\mu(\omega)$ obtained from the experimental results of Kong *et al.* In blue dashed line, the constant μ model with magnetic dipolar correction presented by Draine plus the Eddy currents term. In pink dash-point line, the frequency dependent permeability model plus the Eddy currents term. (b) Enlargement of the short wavelength region where the effect of Eddy currents is noticeable.

ure, where Eddy current including models (blue and pink lines) presents higher extinction values than the rest (red and black lines). All this results are summarized in table 1.

3.2 Eddy currents in core shell particles

The relevance of Eddy currents for particles larger than 20 nm must be taken into account also for multilayer systems. The calculations can be performed as an extension of the method used by Landau. Naming the permeability of each layer ε_i, i=1,2,3 and the radii a, b and c with $a<b<c$, after solving Maxwell equations, the magnetic field in each region depends on the external electric

Table 1 Summary of model comparison. For each particle size d - wavelength λ combination the importance of μ frequency dependence and Eddy currents effects is suggested. In the central circle, the most adequate model is denoted together with its range of validity.

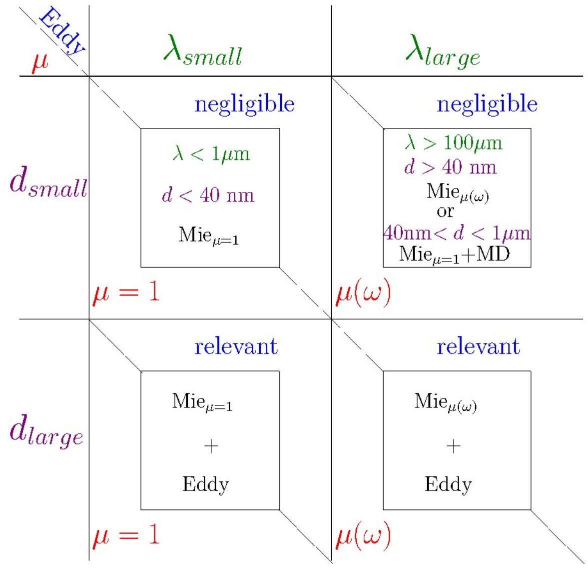

field direction e:[25]

$$\mathbf{H}_i=\left(\frac{f_i'(r)}{r}+k_i^2f_i(r)\right)\mathbf{e}-\left(\frac{3f_i'(r)}{r}+k_i^2f_i(r)\right)(\mathbf{n}\cdot\mathbf{e})\,\mathbf{n} \tag{11}$$

for $i=1,2,3$

$$\mathbf{H}_e=\frac{\alpha}{r^3}\left[3\,(\mathbf{n}\cdot\mathbf{e})\,\mathbf{n}-\mathbf{e}\right]+\mathbf{e} \tag{12}$$

where $f_1=\beta_1\mathrm{sen}k_1r/r$, $f_2=\beta_2\mathrm{sen}k_2r/r+\beta_3\cos k_2r/r$, $f_3=\beta_4\mathrm{sen}k_3r/r+\beta_5\cos k_3r/r$, $f_j'(r)=df_j(r)/dr$ and α is the polarizability. The continuity conditions for the fields at $r=a$ are

$$\frac{f_1'(a)}{a}+k_1^2f_1(a) = \frac{f_2'(a)}{a}+k_2^2f_2(a) \tag{13}$$

$$\frac{3f_1'(a)}{a}+k_1^2f_1(a) = \frac{3f_2'(a)}{a}+k_2^2f_2(a), \tag{14}$$

for $r=b$

$$\frac{f_2'(b)}{b}+k_2^2f_2(b) = \frac{f_3'(b)}{b}+k_3^2f_3(b) \tag{15}$$

$$\frac{3f_2'(b)}{b}+k_2^2f_2(b) = \frac{3f_3'(b)}{b}+k_3^2f_3(b), \tag{16}$$

finally for $r=c$

$$\frac{f_3'(c)}{c}+k_3^2f_3(c) = 1-\frac{\alpha}{c^3} \tag{17}$$

$$\frac{3f_3'(c)}{c}+k_3^2f_3(c) = -\frac{3\alpha}{c^3}. \tag{18}$$

View Article Online
DOI: 10.1039/C6CP08260B

By combining this conditions, the polarizability α can be obtained:

$$\alpha = -\frac{3V}{8\pi}\frac{\beta_{45}\left(z^2\tan z + 3z - 3\tan z\right) + \left(z^2 - 3z\tan z - 3\right)}{\beta_{45} z^2 \tan z + z^2} \qquad (19)$$

$$\beta_{45} = \frac{\left(y_2^2 - y_3^2 + y_2^2 y_3 \tan y_3\right)\left(1 + \beta_{23}\tan y_2\right) + y_2 y_3^2\left(\beta_{23} - \tan y_2\right)}{\left(y_3^2 - y_2^2 + y_2 y_3^2\right)\left(1 + \beta_{23}\tan y_2\right) + y_2^2 y_3 \tan y_2\left(\beta_{23} + \tan y_3\right)} \qquad (20)$$

$$\beta_{23} = \frac{x_1^2 x_2 \tan x_1 \tan x_2 + \left(x_1^2 - x_2^2\right)\tan x_1 + x_1 x_2^2}{\left(x_2^2 - x_1^2\right)\tan x_1 \tan x_2 + x_1^2 x_2 \tan x_1 - x_1 x_2^2 \tan x_2} \qquad (21)$$

where $x_j^2 = \varepsilon_j(\omega a/v_c)^2$, $y_j^2 = \varepsilon_j(\omega b/v_c)^2$ for $j = 1,2,3$, $z^2 = \varepsilon_3(\omega c/v_c)^2$ and v_c is the speed of light.

Figure 4 shows the imaginary part of the specific polarizability of Fe_3O_4 NPs with $R = 500$ nm and $Fe_3O_4@SiO_2@Au$ NPs with magnetite radius $a = 500$ nm and SiO_2 radius $b = 510$ nm for several values of Au radius c. Increasing Au shell thickness shifts the maximum to longer wavelengths with almost no effect in the magnitude (the values are per unit mass of NP). For the naked Fe_3O_4 NPs, $\beta_5 = 0$, so polarizability is reduced to equation 7.

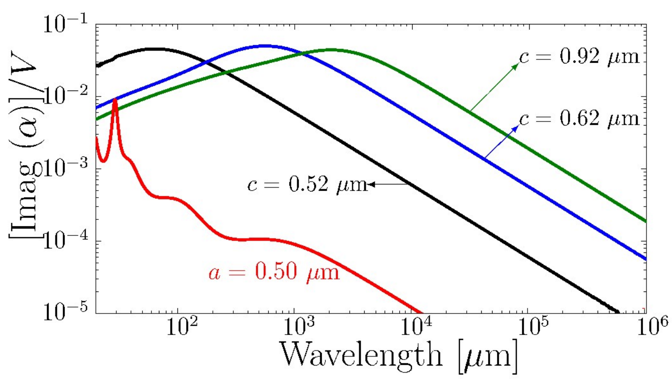

Fig. 4 Imaginary polarizability per unit volume due to Eddy currents in $Fe_3O_4@SiO_2@Au$ NPs for different Au layer thickness. The polarizability maximum shifts to longer wavelengths from the naked 500 nm radius magnetite NP value (red) when adding a 10 nm SiO_2 shell (black).

As shown before, for naked, [20, 500] nm radius magnetite NPs, Eddy currents are relevant for wavelengths shorter than 1 μm. This range of Eddy currents relevance is affected by the thickness of SiO_2 and Au shells, shifting to longer wavelength with increasing thickness.

4 Magnetic NP size determination from optical extinction

As shown in the previous sections, the size distribution of the assembly of particles is a determinant factor in its extinction response. While knowing the size distribution enables the prediction of the extinction spectrum, in the opposite direction the size distribution of the sample can be obtained by fitting the extinction spectrum with the model developed in this work.

4.1 Experimental extinction fitting and size distribution determination of naked magnetite NPs

The extinction spectrum of an aqueous suspension of Fe_3O_4 NPs was obtained in the range [200,700] nm in a Shimadzu 1650 PC spectrophotometer and then fitted with the full Mie theory prediction considering a lognormal size distribution. The obtained mean radius and standard deviation (5.30(15) nm) compare very well with TEM results for a different fraction of the same suspension (4.77(86) nm) as shown in Figure 5.

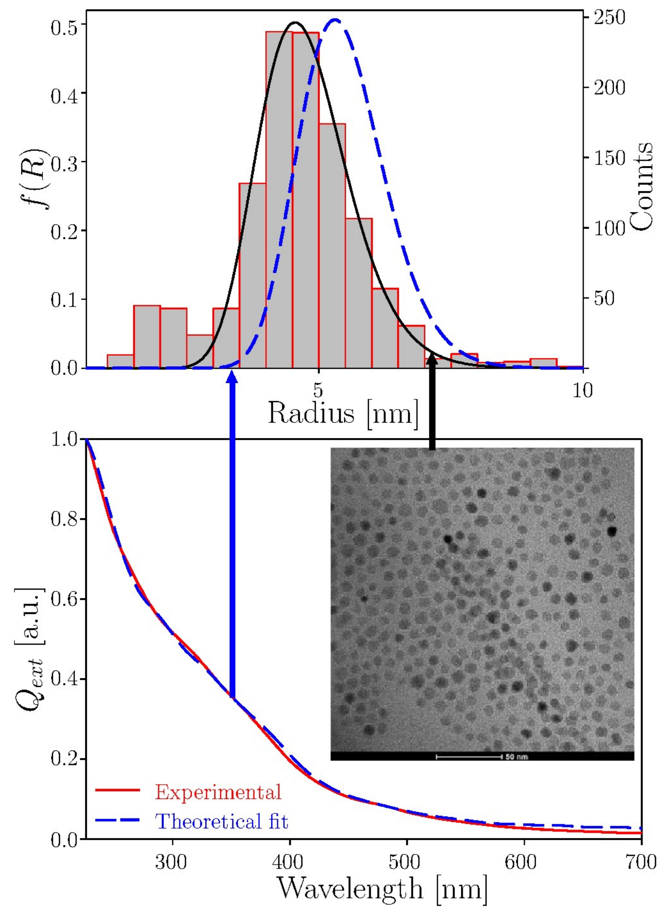

Fig. 5 Top: comparison between fitted TEM size histogram and size distribution from extinction. Bottom: TEM image of the magnetite NPs and experimental extinction spectrum with theoretical fit.

4.2 Core and shell sizing of $Fe_3O_4@Au$ nanoparticles

The same kind of analysis can be performed for core/shell NP. In this case, size distributions of both, core radius and shell thickness are determinant in the optic response of the sample.

- **Effects of core size and shell thickness on plasmon peak**

  In $Fe_3O_4@Au$ NP, a plasmonic peak is present which is the result of the hybridation of the external surface plasmon and the inner cavity plasmon of Au. Figure 6 shows calculated results of extinction spectra with several core-shell size combinations. It can be seen how decreasing the thickness of the shell provoques a narrower, red shifted peak because of the

View Article Online
DOI: 10.1039/C6CP08260B

growing inner cavity influence (Fig. 6a). Core size also affects the ratio between the two plasmons, shifting the peak and changing its contrast (max/min ratio) as shown in figure 6b for NP with 40% shell thickness referred to the core radius.

The size dispersion σ of the cores, calculated as the standard deviation of a lognormal distribution, is another important parameter always present in real systems. Bigger values of σ shift the plasmonic peak to bigger wavelengths and reduce its width (fig. 6c). Due to the asymmetry of the plasmonic peak, we will use the longest wavelength corresponding to 70% of the peak height as a width indicator. In figure 6d, the position of this value is shown for several relative thickness of the shell.

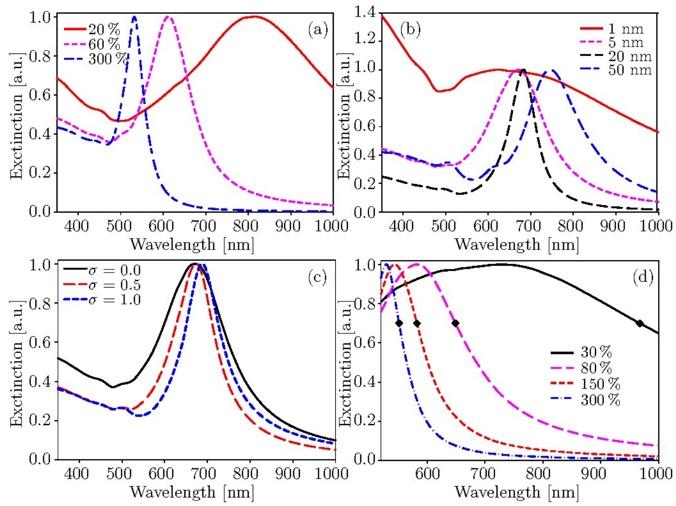

Fig. 6 Extinction spectra for: (a) 4 nm radius Fe_3O_4 core with different values of Au shell relative thickness. (b) different Fe_3O_4 radius with 40% of relative Au shell thickness. (c) 4 nm mean radius Fe_3O_4 core with different dispersion and 40% of relative Au shell thickness. (d) 4 nm radius Fe_3O_4 core with different values of Au shell relative thickness.

- **Graphical determination of core size and shell thickness for Fe_3O_4@Au nanoparticles**

The model presented in this works allows the determinations of the core size and shell thickness of a NP sample from its extinction spectrum via a graphic method.

Figure 7 a and b are colour maps for peak and 0.7 of peak positions respectively in function of core size and relative shell thickness. Since a given peak position or peak width can be the result of several core/shell radius combinations, the plasmon peak and peak width values obtained from an experimental extinction spectrum are represented by contour lines in the corresponding map of the figure. Superimposing peak and 0.7 of peak contour lines, the core and shell radii of the sample is given by the intersection.

Two determination examples are shown together in figure 9 using optical extinction data reported by Lingyan *et al* for two samples of different mean size (*a* particles and *b* particles).[26] The results are compared in table 2 with TEM sizes reported in the original work.

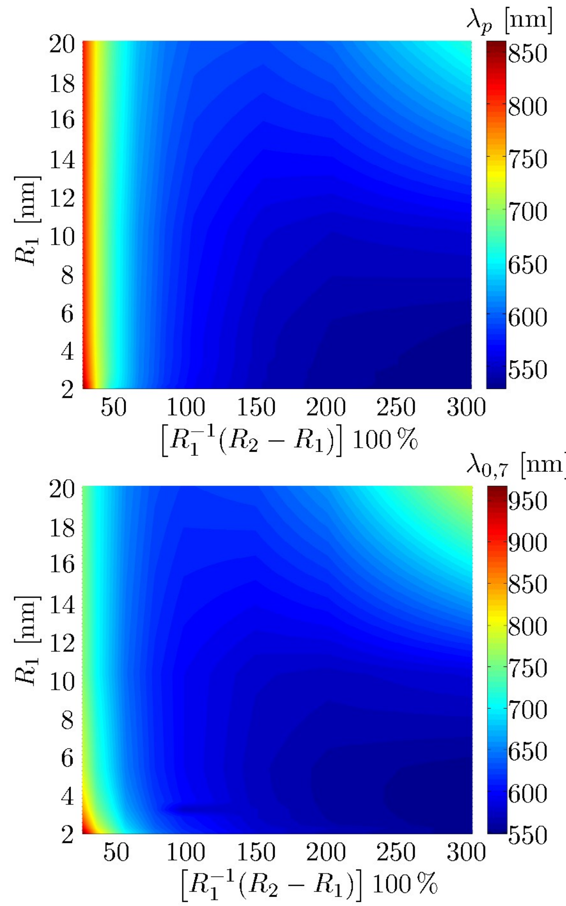

Fig. 7 Top: Plasmonic peak position wavelength (colour scale) in function of core radius R_1 and relative shell thickness $100*(R_2-R_1)/R_1$. Bottom: 0.7 of peak wavelength in function of core radius R_1 and relative shell thickness $100*(R_2-R_1)/R_1$.

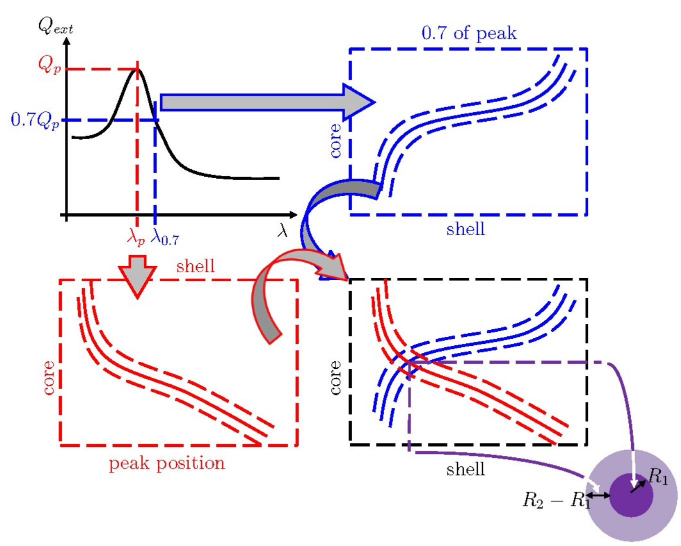

Fig. 8 Scheme of sizing method. Peak and 0.7 of peak wavelengths from the experimental spectrum correspond to a contour line each in the corresponding map of core radius versus relative shell thickness. The graphical interception between this lines indicates the modal values of the sample.

View Article Online
DOI: 10.1039/C6CP08260B

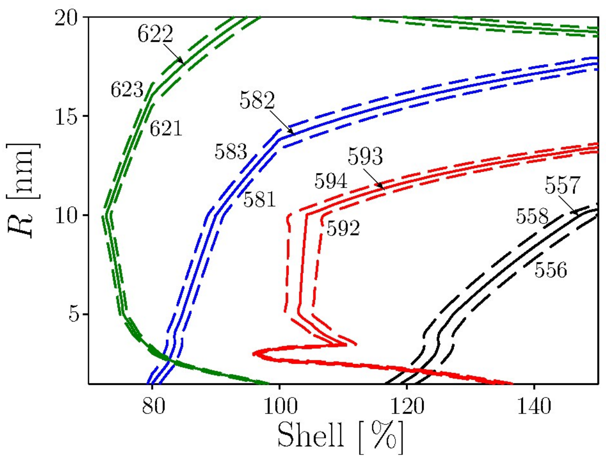

Fig. 9 Contour lines for peak and 0.7 of peak wavelength positions for a (black for peak, red for 0.7 of peak) and b (blue for peak, green for 0.7 of peak) particles experimental extinction spectra. Vertical and horizontal position of the intersection between each pair of curves corresponds to the core and shell radius of the sample respectively. Lateral dashed lines represent error bars of the experimental values.

Table 2 Internal (R_1) and external (R_2) radii of a and b particles from TEM and optical extinction.

	Optical extinction	TEM
R_{1a}(nm)	2.14	2.25
R_{2a}(nm)	4.75	3.40
R_{1b}(nm)	2.70	2.70
R_{2b}(nm)	4.93	3.50

The solution given by the intersection of the contour lines is unique only if the size distribution of the sample is unimodal, which is the most common scenario. Multimodal distributions will return several intersections points.

4.3 Fe_3O_4@SiO_2@Au three layer nanoparticles

Three layer Fe_3O_4@SiO_2@Au nanoparticles present also a combination of useful magnetic and optical properties arise by well separated wavelength ranges. Being the optical and magnetic responses more intense with bigger quantities of Au and Fe_3O_4 respectively, there exist a compromise between core size and shell thickness for a given final diameter. Figure 10 shows results of the numeric calculations for 3 layer Fe_3O_4@SiO_2@Au NPs with several values of magnetite radius R_1 and Au shell external radius R_3, while fixing the SiO_2 external radius in $R_2 = 20nm$.

As shown in the Figure 10, increasing the size of the magnetite core (*ergo* decreasing the SiO_2 shell thickness T since $R_2 = R_1 + T$ =20 nm in all cases) provokes a diminution in the intensity of the extinction peak in the same way as the core-shell particles. This effect is present for all values of Au thickness R_3. On the other hand, changing the Au shell thickness affect both, the position and the width of the plasmonic peak since the plasmon itself is originated in the metal layer.

5 Conclusions

Theoretical extinction spectra of Fe_3O_4, Fe_3O_4@Au and Fe_3O_4@SiO_2@Au spherical NPs were calculated from Mie theory,

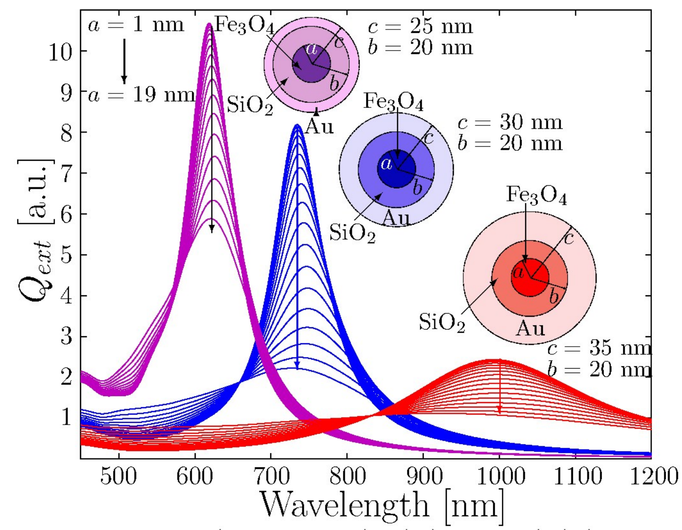

Fig. 10 Calculated extinction peaks of Fe_3O_4@SiO_2@Au particles for several values of core radius and Au shell thickness.

taking into account the wavelength dependencies of both electric permittivity and magnetic permeability. The effects on the magnetic polarizability of Eddy currents induced by the incoming electromagnetic wave were also introduced in the calculations. Reported experimental microwave permeability values of MNPs were used, together with Gilbert equation and Bruggermann effective medium theory, in order to determine the so called Gilbert parameter α_G needed for full range calculation of the magnetite permeability. To the best of our knowledge, this information was not available in literature before.

As expected, the results indicate that dipolar interaction magnetic response of the considered multilayer NPs is negligible in the UV-Vis-NIR wavelength range. For NPs smaller than 500 nm, Mie theory with $\mu = 1$ plus a magnetic dipolar contribution may be used instead of Mie with $\mu(\omega)$ yielding identical results. This behaviour can be understood considering the magnetic relaxation process undergone by NPs in that size range: the implied relaxation time constants are several orders of magnitude larger that the period of the incident wave. On the other hand, the comparison between models indicate that Eddy contribution must be taken into account when calculating extinction spectra for magnetite NPs sizes larger than 40 nm at short wavelengths. This is a remarkable result since magnetic related effects are usually neglected in the UV-Vis-NIR range.

The developed model was applied to retrieve the size distribution of a magnetite NPs suspension from its optical extinction spectrum. The very good agreement with TEM results supports the correctness of the approach. This method presents an interesting sizing alternative with several advantages over local probe techniques such as TEM and SEM: the equipent needed is readly available in any laboratory, the measurement are simple and non destructive and principally, the sample can be observed in its native suspension state with saturated statistic.

Additionally, a novel graphical method for determining modal sizes of core and shell multilayer NPs was developed. The deter-

View Article Online
DOI: 10.1039/C6CP08260B

mination is based on finding the intersection of level curves for plasmon resonance maximum position and width versus core and shell radii. This method was tested comparing with experimental TEM results from two samples of low size dispersion Fe_3O_4@Au NPs prepared by chemical methods. While there is an excellent agreement between techniques for core radius, the shell thickness obtained by the optical method was 1.4 times larger for both samples. This discrepancy could be originated by the neglecting of a possible penetration of the Au conduction electrons in the magnetite core. Otherwise that, in the case of naked magnetite NP where no penetration is present, the relation between TEM and optical radii is similar to the latter. Therefore, the discrepancy could be instead caused by the influence on the effective external radius of a differentiated water layer or a non crystallinity of the outer NP layer.

Summarizing, this work presents for the first time a complete formulation of the extinction properties for magnetic core, single and multilayer NPs, through the utilization of full Mie theory with frequency dependent permeability, together with Eddy currents contribution. The power of this model was demonstrated by its application for both, experimental sample characterization and theoretical prediction of optical properties for a wide range of multilayer NPs assemblies. Extension of this model and its application to other configurations is in due course.

6 Acknowledgments

This work was granted by PIP 0280 of CONICET, PME2006-00018 of ANPCyT, grant 11/I197 of Facultad de Ingeniería, UNLP. D. C. Schinca is Member of Comisión de Investigaciones Científicas de la Provincia de Buenos Aires (CICBA), Argentina. L. B. Scaffardi,is researcher of CONICET. Igancio J. Bruvera is postdoctoral fellow of CONICET and L. J. Mendoza Herrera is PhD fellows of CONICET, Argentina.

References

1 Q. A. Pankhurst, J. Connolly, S. K. Jones and J. Dobson, *Journal of Physics D: Applied Physics*, 2009, **136**, R167.
2 E. C. Dreaden, A. M. Alkilany, X. Huang, C. J. Murphy and M. A. El-Sayed, *Chem. Soc. Rev.*, 2012, **41**, 2740–2779.
3 L. Dykman and N. Khlebtsov, *Chem. Soc. Rev.*, 2012, **41**, 2256–2282.
4 M. Agotegaray, S. Palma and V. Lassalle, *Journal of nanoscience and nanotechnology*, 2014, **14**, 3343–3347.
5 I. J. Bruvera, R. Hernąndez and G. F. Mijangos, C.and Goya, *Journal of Magnetism and Magnetic Materials*, 2015, **377**, 446–451.
6 A. S. Pereyra, O. Mykhaylyk, E. F. Lockhart, J. R. Taylor, O. Delbono, R. G. Goya, C. Plank and C. B. HereÃśu, *Journal of Nanomedicine Nanotechnology*, 2016, **7**, 2.
7 C. M., M. O., B. P., O. J., S. B., W. S., K. FE., P. C., S. BB. and F. TA., *Nanomedicine*, 2016, **11**, 1787–1800.
8 O. Bomati-Miguel, N. Miguel-Sancho, I. Abasolo, A. P. Candiota, A. G. Roca, M. Acosta, S. Schwartz, C. Arus, C. Marquina, G. Martinez and J. Santamaria, *Journal of Nanoparticle Research*, 2014, **16**, 1–13.
9 H. B. Na, I. C. Song and T. Hyeon, *Advanced Materials*, 2009, **21**, 2133–2148.
10 B. Thiesen and A. Jordan, *International journal of hyperthermia*, 2008, **24**, 467–474.
11 Y.-H. Deng, C.-C. Wang, J.-H. Hu, W.-L. Yang and S.-K. Fu, *Colloids and Surfaces A: Physicochem. Eng. Aspects*, 2005, **262**, 87–93.
12 S. Santra, R. Tapec, N. Theodoropoulou, J. Dobson, A. Hebard and W. Tan, *Langmuir*, 200, **10**, 2900–2906.
13 E. Taboada, R. Solanas, E. Rodríguez, R. Weissleder and A. Roig, *Advanced Functional Materials*, 2009, **19**, 2319–2324.
14 C. A. Ballesteros, J. Cancino, V. S. Marangoni and V. Zucolotto, *Sensors and Actuators B: Chemical*, 2014, **198**, 377–383.
15 Y. L., Z. Y., C. R., Z. D., W. X., C. F., W. J. and X. M., *Talanta*, 2015, **131**, 475–479.
16 M. M., K. S., G. SK., P. S., S. TK., Y. SM. and P. T., *J Colloid Interface Sci.*, 2005, **286**, 187–194.
17 K. A. Mahmoud, E. Lam, S. Hrapovic and J. H. T. Luong, *ACS Applied Materials & Interfaces*, 2013, **5**, 4978–4985.
18 I. Y. Goon, L. M. H. Lai, M. Lim, P. Munroe, J. J. Gooding and R. Amal, *Chemistry of Materials*, 2009, **21**, 673–681.
19 B. T. Draine and B. Hensley, , 2013, **765**, 159.
20 D. O. Smith, *Phys. Rev.*, 1956, **102**, 959–963.
21 S. Chikazumi, *Physics of magnetism*, John Wiley & Sons, New York, 1st edn, 1964.
22 I. Kong, S. H. Ahmad, M. H. Abdullah, D. Hui, A. N. Yusoff and D. Puryanti, *Journal of Magnetism and Magnetic Materials*, 2010, **322**, 3401–3409.
23 D. Rousselle, A. Berthault, O. Acher, J. P. Bouchaud and P. G. Zérah, *J. Appl. Phys.*, 1993, **74**, 475.
24 L. Z. Wu, J. Ding, H. B. Jiang, C. P. Neo, L. F. Chen and C. K. Ong, *Journal of Applied Physics*, 2006, **99**, 083905.
25 L. D. Landau and E. Lifshitz, *Electrodynamics of Continuous Media*, Pergamon Press, New York, 2nd edn, 1960.
26 W. Wang, L. Jin, F. Quan, S. Masatsugu, S. I. S., E. M. H., L. Yuehe, K. Nam, W. J. Q. and Z. Chuan-Jian, *The Journal of Physical Chemistry B*, 2005, **109**, 21593–21601.